Author's Accepted Manuscript

www.elsevier.com/locate/talanta

Saccharomyces-derived carbon dots for biosensing pH and vitamin B 12

Ying Yu, Chunguang Li, Cailing Chen, He Huang, Chen Liang, Yue Lou, Xiao-Bo Chen, Zhan Shi, Shouhua Feng

PII: S0039-9140(18)31161-5
DOI: https://doi.org/10.1016/j.talanta.2018.11.010
Reference: TAL19243

To appear in: *Talanta*

Received date: 27 August 2018
Revised date: 31 October 2018
Accepted date: 4 November 2018

Cite this article as: Ying Yu, Chunguang Li, Cailing Chen, He Huang, Chen Liang, Yue Lou, Xiao-Bo Chen, Zhan Shi and Shouhua Feng, Saccharomyces-derived carbon dots for biosensing pH and vitamin B 12, *Talanta,* https://doi.org/10.1016/j.talanta.2018.11.010

Saccharomyces-derived carbon dots for biosensing pH and vitamin B 12

Ying Yu[a] , Chunguang Li[a,*] , Cailing Chen[a] , He Huang[a] , Chen Liang[a] , Yue Lou[a] , Xiao-Bo Chen[b] , Zhan Shi[a*], Shouhua Feng[a]

[a]State Key Laboratory of Inorganic Synthesis and Preparative Chemistry, Jilin University, Changchun 130012, People's Republic of China

[b]School of Engineering, RMIT University, Carlton, VIC 3053, Australia

cglee@jlu.edu.cn

zshi@mail.jlu.edu.cn

***Corresponding authors.** Fax: +86-85168624.

Abstract

Photoluminescence(PL) nano-biosensors that can be used for accurately and reliably monitoring pH and vitamin hold a great promise in biology and medicine. Herein, a high quantum yield of 16% saccharomyces-derived N-doped carbon dots (s-N-CDs) was synthesized through a simple and one-pot microwave-assisted hydrothermal approach. The produced s-N-CDs are an excellent multi-functional biosensor for the applications of pH sensing and vitamin probing. Fluorescence intensity and fluorescence lifetime dramatically increases with pH decreasing from 14 to 2. Moreover, the fluorescence intensity presents highly reversible abilty from 13 to 2 without any profound attenuation after ten consecutive circles. More importantly, the CDs prepared herein are sound option for assaying cobalamin (VB 12) based fluorescence resonance energy transfer (FRET) with a superior low detection limit of 2.19 μM.

Graphical abstract

fx1

Keywords

Saccharomyces; Carbon dots; biosensor; pH; vitamin B 12

1. Introduction

Biosensor is an analytic device consisting of a biological unit and a selective detector to convert biological responses into electronical signals[1]. Owing to its superior selectivity, high sensitivity, fast analysis, and low-cost features, biosensor has attracted ample interest from both academia and industry over the past decades[2-6]. It is well recognized that different biological organs, tissues and cells have their specific survival pH ranges in the human body. As such, it is of great importance to enable reliable and accurate monitoring of organs and intracellular pH values[7-8]. In addition, some elements in the human body also play a crucial role in human health. For instance, Vitamin B protects our livers against excess alcohol intake[9]. When the deficiency in supplies of such key vitamins takes place, acute or chronical damages may be incurred to liver[10]. Therefore, development of an accurate monitoring system regarding vitamins supplies is highly desired.

To address such technical issues, the prevalent option is non-contact sensor, in particular fluorescence sensor that exhibits a broad range of applications in recent years. The fluorescence intensity or fluorescence life changes are a key indicator of some biological activities of organism[11]. A larger number of nanomaterials have been produced as biosensor components, such as, functionalized CdS quantum dots for probing tumor cells[12], and AuC@urease nanoparticles for selective detection of urea in blood[13], organic fluorescent

molecules used for analysing amyloid beta aggregates[14]. These sensor components are mainly consisted of organic fluorescent molecules or semiconductor quantum dots. However, severe concerns were raised over the safety of such nanosize materials in physiological environment[15, 16].

Carbon dots (CDs) are an emerging material for such biosensor device, which outperform other nanomaterials in low toxicity[17], high cost-effectiveness[18-22] and strong photoluminescence[23-25]. CDs are defined as well dispersed, spherical, spherical fluorescent carbon nanoparticles of less than 10 nm in diameter[26]. A variety of synthetic approaches have been proposed for CDs, including top-down strategies of arc discharge[27], laser ablation[28] and electrochemical oxidation[29], and bottom-up techniques of combustion[30], hydrothermal treatments[31] and pyrolysis[32]. Heteroatoms can also be doped with CDs to perform functions for various needs. Though research on CDs has been boosted in a larger number of practical applications in recent years[33-39]. It is challenging to develop a simple, rapid and cost-effective approach to synthesize CDs with a high yield rate for mass production.

Herein, we prepare N-doped fluorescent CDs with several cheap and green non-toxic fungus biomass raw materials (*i.e.* saccharomyces, lactobacillus, bacillus brevis, bacillus lateraporus and brevibacterium) and ethylenediamine in the role of water solvent through a one-shot microwave-assisted method. To employ the superior photoluminescence of saccharomyces synthesized CDs (s-N-CDs) for biosensing applications, the preparation, properties and applications of s-N-CDs are systematically studied in this paper. The prepared s-N-CDs perform a multifunctional role in detecting both pH variations and concentration of Vitamin B 12 in a selective way with a high resolution. Our results could provide new guidance for the design and development of functional CDs for the next generation of high-performance photoluminescence-based biosensor devices.

2. Material and methods

2.1. Materials

Ethylenediamine was purchased from Shanghai Sinopharm Chemical Reagent Co. Ltd., China. Saccharomyces, lactobacillus, bacillus brevis, bacillus lateraporus, brevibacterium were purchased from Shandong Sukahan Co. Ltd. Cobalamin, biotin, pyridoxine, calpanate, nicotinic acid, thiamine hydrochloride, were purchased from Shanghai energy chemical Co. Ltd., China. $CdCl_2$, $CrCl_3$, $CuCl_2$, $FeCl_3$, KCl, NaCl, $NiCl_2$, $PbCl_2$, glycine, L-alanine, L-threonine and L-serine are purchased from Sigma-Aldrich, Ltd. Dialysis bags were purchased from Shanghai Yuanye Bio-Technology Co. Ltd., China.

2.2. Methods

2.2.1. N-doped CDs

Water-soluble N-CDs were prepared through a one-pot microwave hydrothermal method. Typical steps of experiment are described as follows: saccharomycetes (0.4000 g) and ethanediamine (5 mL) were dissolved in deionized water (15 mL). Then, the mixture was transferred to a microwave oven(ETHOS ONE, ITALY), and heated up to and held at 200 °C for 3 h. After naturally cooling down to room temperature, raw products were obtained. Finally, after dialyzing (MW = 500-1000) for 24 hours, the s-N-CDs solution was obtained. (The other four types bacteria-derived CDs were produced through the same synthetic procedures).

2.2.2. pH probing

A certain quantity of NaOH or HCl solution was added into 1 mL dialyzed s-N-CDs solution. Values of pH were read with pH meter. Fluorescence spectra and fluorescence lifetime of s-N-CDs solution with varying pH values (1-14) (λ_{em} = 460 nm, λ_{ex} = 380 nm) were recorded through a spectrofluorophotometer.

2.2.3. Vitamin detection

Two mL dialyzed s-N-CDs solutions was diluted with 1 mL phosphate buffered saline (PBS, pH = 7.4). Various vitamins B (VB 1, VB 3, VB 5, VB 6, VB 7, VB 12), common metal cations and amino acid of 1 mM were added into the above diluted s-N-CDs solution, respectively and the corresponding fluorescence intensity was measured. For the detection of VB 12, a number of concentrations of VB 12 (0, 10, 20, 30, 40, 50, 60, 70, 80, 90, 100 μM) were mixed with the s-N-CDs solution, and the respective responsive fluorescence spectra were recorded (λ_{ex} = 380 nm).

2.2.4. Characterization

TEM images were obtained by using an FEI Tecnai G2 S-Twin microscope with a field-emission gun operated at 200 kV. FTIR spectra were recorded with a Bruker IFS 66v/S FTIR spectrometer. Ultraviolet-visible (UV−vis) absorption spectra were measured with a Shimadzu UV-2450 UV-vis spectrophotometer. X-ray diffraction (XRD) were carried out on a Rigaku D/Max 2500 diffractometer with a graphite monochromator using Cu Kα radiation operating at 200 mA and 40 kV. X-ray photoelectron spectroscopy (XPS) was conducted on an ESCALAB 250 spectrometer with a mono X-ray source with Al Kα excitation (1486.6 eV). Binding energy calibration was based on C 1s at 284.7 eV. Fluorescence emission and excitation spectra of the products were measurand with an Edinburgh Instruments FLS 920.

2.2.5. Fluorescence lifetime measurements

The fluorescence lifetime of the resultant s-N-CDs were measured by the following equation:

$$Y(t) = A_1\exp(-t/s_1) + A_2\exp(-t/s_2),\ A_1+A_2=1$$

Where s_1, s_2 are decay time constants[40]. A_1 and A_2 stand for the percentage of s_1 and s_2 in total decay lifetime.

$$\tau=A_1t_1^2+A_2t_2^2 / (A_1t_1+A_2t_2)$$

Where τ is the average lifetime of the photoluminescence decay[41-43].

3. Results and discussion

3.1. Synthesis and characterization of the N-doped C-dots

We have demonstrated that microwave-assisted hydrothermal conditions facilitate the growth of N-doped CDs (N-CDs). Five distinct carbon sources (*i.e.* saccharomyces, lactobacillu, bacillus brevis, bacillus lateraporus and brevibacterium) were employed to react with ethylenediamine in water at 200 °C for 3 h, respectively. Of these, the N-CDs made from saccharomyces exhibited excellent photoluminescence properties and a narrow size distribution range, which is the research focus in the following parts. Morphology, structure and size distribution of s-N-CDs were characterized by TEM (Fig. 1a). In general, the s-N-CDs displaying a spherical or nearly spherical shape were well-dispersed with an

average diameter of 2.9 nm based on no less than 200 measurements of individual nanoparticles (Fig. S1, ESI†). TEM images (Fig. S2, ESI†) indicate that the same type of carbon source also synthesized small size carbon dots. XRD pattern (Fig. 1b) exhibits a typical broad peak at 24.9°, which is attributed to the diffraction of the (002) lattice plane[44]. Two broad peaks at 1360 cm^{-1} and 1580 cm^{-1} could be seen from Raman spectrum (Fig. 1c), which are in correspondence to D band (sp^3- hybridized) and G band (sp^2-hybridized), respectively. The most intensive peak is D1 band, which appears at 1360 cm^{-1} and corresponds to a graphitic lattice vibration mode with A_{1g} symmetry. The G (''Graphite'') band at around 1580 cm^{-1} corresponds to an ideal graphitic lattice vibration mode with E_{2g} symmetry[38]. It is proved that s-N-CDs have a certain degree of graphitization. Moreover, FTIR spectra of s-N-CDs and saccharomycetes (Fig. 1d) reveal that a strong absorption band centered at about 3295 cm^{-1} is assigned to the stretching vibrations of N-H or O-H[45]. The absorption peaks located at 1550 cm^{-1} and 1423 cm^{-1} may attribute to the Amide II bending and C-N stretching, respectively[39]. The existence of carboxylic groups can be proved by the =C–H bending for trans at 997 cm^{-1} and C=O stretching at 1659 cm^{-1}[46].

XPS characterization (Fig. 2a) demonstrates that C (291.6 eV), N (399.7 eV) and O (531.6 eV) are the main elements of s-N-CDs, Si and S are the minor. Si 2p peak at 101.8 eV is assigned to the presence of four-valent silicon (Si–O/Si–C). S 2p peak at 407.0 eV is attributed to the presence of C–SOx. The three fitted peaks at 284.7, 286.0 and 287.9 eV in C 1s spectrum (Fig. 2b) can be attributed to C–C/C=C (sp^2 carbons), C–O/C–N (sp^3 carbons) and C=O, respectively[47]. The peaks of N 1s spectrum (Fig. 2c) located at 399.7 eV correspond to C-N-C and 401.3 eV are assigned to N-H. O 1s spectrum (Fig. 2d) indicates the presence of C=O and C-O, respectively. These results demonstrate that s-N-CDs are composed of abundant elements and surface-modified with various functional groups (carboxyl, amino, hydroxyl, imino and amide bonds), which agrees with FTIR results (Fig. 1d). UV-vis absorption spectrum (Fig. 3a) displays a broad absorption band with peaks centered at 281 nm (carbonic corecentre) and 340 nm (surface/molecule center). Due to the Mie scattering of nanosize particles, high energy tail in visible region occurs[48]. Inset of Fig. 3a depicts the s-N-CDs exposed to daylight (left) is colorless while exhibits a bright blue color under UV light (λ_{ex} = 365nm, intermediate). s-N-CDs are feasible fluorescent inks for printing with sharp and visible patterns. As the excitation wavelength increases from 260 to 480 nm, the emission peak shifts towards red zones (Fig. 3b). This excitation dependent fluorescence behavior may be attributed to the wide distribution of differently sized s-N-CDs and surface chemistry or different emissive traps[11, 27-29]. The other CD couterparts have similar properties (Figs. S3 and S4, ESI†). s-N-CDs have an absolute quantum yield of up to 16%, whilst the other four N-CDs also have desirable optical properties. (Table. 1, ESI†). The calculated CIE (Fig. 3c) corresponds to the emission diagram (Fig. 3b) with an excitation wavelength number at 380 nm and an emission wavelength number at 460 nm**.** To elucidate the fluorescence mechanism of s-N-CDs, fluorescence lifetime measurement was performed (Fig. 3d) and the average lifetime is 6.84 ns. The decay curve can be fitted to biexponential functions Y(t) based on nonlinear least-squares analysis.

To evaluate their potentional for the expected applications in vivo, we investigated the influence of UV irradiation, temperature and ionic strength on the fluorescence stability of s-N-CDs. To study the anti-bleaching performance, s-N-CDs solutionwas placed under UV irradiation (λ_{ex} = 365 nm) for 30 min, during which the fluorescence intensities of the s-N-CDs solution were recorded every 30 s. No significant changes in color of the s-N-CDs (Fig. 4a) and only a slight variation in the corresponding photostability (Fig. 4b) were indentified, which indicates an excellent anti-bleaching ability of s-N-CDs. P is the fluorescence intensity per measurement. P_0 is the original fluorescence intensity which is measured at 25 °C, pH = 7.4 and not irradiated by the UV lamp. (All of the P_0 covered in this paper is at the same condition).

Similarly, to touch the base of temperature effect, fluorescence intensity of s-N-CDs solution was recorded at an interval of 8 °C (2 – 80 °C). As shown in Fig. 4c, the location of the fluorescence emission peak remains and the fluorescence intensity of the corresponding color is changed slightly with increasing temperature. Photostability study (Fig. 4d) shows that s-N-CDs have a desirable thermal stable ability. To investigate the ionic strength effect, fluorescence intensity of s-N-CDs solution was recorded every 100 mM (0 - 1 M). The fluorescence intensity was substantially unchanged (Fig. 4e) and no drops are seen in the corresponding photostability on the whole (Fig. 4f), which indicates that photoluminescence intensity of the s-N-CDs is not independent of ionic strength of the solution. s-N-CDs maintain a high degree of stability in a variety of environments, suggesting a strong potential for practical applications in vivo.

3.2. Fluorescence responses of s-N-CDs towards pH

It is evident that fluorescence intensity and fluorescence lifetime are closely correlated with pH of the s-N-CDs solutions. As shown in Fig. 5a, when pH of s-N-CDs solutions decrease from 14 to 2, fluorescence intensity increases a lot, but fluorescence emission peak position remains unchanged. There is a large color difference between the s-N-CDs of pH = 13 and pH = 2 under 365 nm irradiation (Fig. 5b). Furthermore, the reversibility of such a pH-switched operation is reproducible. As shown in Fig. 5 (c) and (d), pH values of s-N-CDs solutions can be adjusted cycling from pH = 2 to pH = 13 using HCl and NaOH, and the fluorescence switching operation can be repeated over ten consecutive cycles without profound fluorescence degradation. The strong optical responses to pH variations of s-N-CDs solutions, may be attributed to the protonation-deprotonation of the surface state with amide and carboxyl groups, under acidic conditions, where s-N-CDs exist as non-aggregated and dispersed substances. However, under alkaline conditions s-N-CDs may aggregate due to the formation of intermolecular hydrogen bonds, and lead to fluorescence quenching[49, 50].

Fluorescence lifetimes as a function of temperature (2-80 °C) and pH were evaluated to clarify the optical responses of s-N-CDs to the changes of temperature and pH (Fig. 6a-c). A constant fluorescence lifetime emerges with increasing temperature. In contrast, the s-N-CDs exhibit extraordinary performance as a fluorescence lifetime-based pH sensor (Fig. 6d-f). When pH value of s-N-CDs solutions is adjusted from 1 to 14, fluorescence lifetime decreases from 14.00 to 6.01 ns. Obviously, the fluorescence lifetimes of s-N-CDs are selective and sensitive to pH. It should be noted that there will be good prospects for nanoprobes based on fluorescent decay kinetics.

Especially in the fields of biology and medicine, specific treatments may be achieved depending on the pH value of the environments.

To examine the potential application of the s-N-CDs for imaging and pH sensing in living cells, the laser confocal microscopic images of A549 cells were carried out. As shown in Fig. 7, blue fluorescence emissions from s-N-CDs was found from A549 cells at a 405 nm excitation. Furthermore, s-N-CDs-stained A549 cells exhibit strong blue fluorescence at pH 6.0 (Fig. 7a), whereas the fluorescent brightness obviously reduces as the pH increases (Fig. 7b and c). In order to compare the pH sensing capabilities in different cell types, LO2 and HepG2 cells were also tested (Fig. S5, ESI†). It turns out that the fluorescence intensity decreased with increasing pH in both A549, LO2 and HepG2 cells. These results successfully demonstrate that the s-N-CDs can serve as a promising probe for the potential application in intracellular pH sensing. More importantly, it is clearly seen that after incubating HepG2 cells in s-N-CDs at pH 6, brighter fluorescence images were obtained by exciting at 405 nm than LO2 cells. This phenomenon may be caused by the weakly acidic microenvironment of tumor cells and their stronger phagocytic capacity [51]. This study provides a useful approach for the development of unique carbon dots for facilitating specific biological sensing.

3.3. Sensitive and selective detection VB 12

Vitamin is essential to maintain the normal function of the human body, and plays an important role in regulating the essential activities of many enzymes in metabolism[46]. For this purpose, it is imperative to detect and monitor Vitamin content in the human blood serum. In this research, highly water soluble s-N-CDs with high fluorescence stability were synthesized as a novel fluorescence-based nanoprobe. Fig. 8 (a) shows normalized color plots of fluorescence spectrum of the s-N-CDs with various vitamins, such as VB 1, VB 3, VB 5, VB 6, VB 7 and VB 12. In comparison to other vitamins, VB 12 plays a strong quenching role in fluorescence intensity, which confirms good selectivity of the s-N-CDs based sensor. And corresponding fluorescence spectra is shown in Fig. 8 (b). A rational mechanism was proposed herein to attribute to the fluorescence-intensity quenching role of VB 12 on a basis of the good matching of UV-Vis absorption spectrum of VB 12 with the emission spectrum of s-N-CDs (Fig. S6, ESI†). We therefore speculates that there is a fluorescence resonance energy transfer process between s-N-CDs and VB 12 due to the overlap of the emission spectrum of the s-N-CDs and the UV-vis absorbance spectrum of VB 12. This reasonable assumption does fit well with the previous literature[9]. To eliminated the potential interfering specie/factors, the effect of the fluorescence intensity ratio of the s-N-CDs were studied after their exposure to other common metal cations and amino acid with the same detection condition as that of the VB 12. (Fig. S7, ESI†)

To monitor the detection sensitivity of s-N-CDs, normalized color plots of fluorescence spectrum of s-N-CDs solutions containing various concentrations (10-100 μM) of VB 12 are presented in Fig. 8 (c) and the corresponding fluorescence spectra are presented in Fig. 8 (d). The increasing concentration of VB 12 leads to linearly decreasing fluorescence intensity. A Stern-Volmer formula ($I_0/I = Kq[Q] + C$) is employe to evaluate the quenching effect of VB 12. I_0 is the fluorescence intensity in the absence of VB 12 and I is the fluorescence intensity in the presence of VB 12. Kq is the fluorescence quenching constant and [Q] is the concentration of VB 12. There is a good linear relationship (R^2=0.97542) of I_0/I against the concentration of VB 12 (Fig. S8 ESI†). The intercept is C and slope is Kq. The limit of detection (LOD) could be obtained

by the formula (3σ/S, where S is Kq and σ is the standard deviation) [52, 53]. The measurements reveal Kq of 0.02277, σ of 0.0166 and calculated LOD of 2.19 μM, repsectively. Such a superior low limit of detection demonstrates a high VB 12-detecting sensitivity of the s-N-CDs.

4. Conclusion

Highly fluorescent and water-soluble N-doped carbon dots are synthesized by a simple and environmentally-friendly approach with saccharomycetes as precursor and ethanediamine as nitrogen source. N-doped carbon dots are consisted of desirable functional groups and display excellent photoluminescent properties. Such carbon dots can serve as fluorescent nanosensor to detect pH. When pH changes from 14 to 2, fluorescence intensity and lifetime of s-N-CDs increase significantly, but conversely, fluorescence intensity decreases sharply, and generates an "switch on-off-on" loop that can be repeated over ten cycles. This contact-less pH fluorescence sensor shows a great potential in future biological and medical applications. More importantly, the N-doped carbon dots are employed for assaying VB 12. In several kinds of the B vitamins, common metal cations and amino acid, VB 12 can be detected specifically, and a LOD as low as 2.19 μM is realized. Compared with the FRET optical sensors based on other quantum dots, our sensor has lower cytotoxicity and greater probability in detecting VB 12 in vivo.

Acknowledgments

Funding:

This work was supported by the Foundation of the Natural Science Foundation of China (nos. 21771084, 21771077 and 21621001), the National Key Research and Development Program of China (no. 2016YFB0701100), the 111 project (no. B17020), the S&T Development Program of Jilin Province of China (no. 20160101325JC). The authors also gratefully acknowledge the financial support by Program for JLU Science and Technology Innovative Research Team (JLUSTIRT).

Author contributions:

Author contributions: Z.S. and C.L. supervised and coordinated all aspects of the project. S.F. also coordinated this work. Y.Y. designed and wrote the paper. C.C. did part of the experiments. H.H. related part of the analyses. C.L. and Y.L. performed TEM measurements. X.C. assisted in the analysis of the data. Z.S. and C.L. revised the manuscript. All authors discussed and commented on the manuscript. **Author Agreement/Declaration：**

All the authors have read and approved this version of the article, and due care has been taken to ensure the integrity of the work. No part of this paper has been published elsewhere. Competing interests: The authors declare that they have no competing interests. Data and materials availability: All data needed to evaluate the conclusions in the paper are present in the paper and/or the Supplementary Materials. Additional data related to this paper may be requested from the authors.

References

[1] K. Su, J. Zhou, L. Zou, T. Wang, L. Zhuang, N. Hu and P. Wang, Integrated multifunctional cell-based biosensor system for monitoring extracellular acidification and cellular growth, Sens. Actuators, A., 220(2014) 144-152.

[2] Z. Guo, L. Murphy, V. Stein, W.A. Johnston, S. Alcala-Perez, K. Alexandrov, Engineered PQQ-Glucose Dehydrogenase as a Universal Biosensor Platform, J. Am. Chem. Soc., 138(2016) 10108-11.
[3] W. Liu, H. Dong, L. Zhang, Y. Tian, Development of an Efficient Biosensor for the In Vivo Monitoring of Cu^{+} and pH in the Brain: Rational Design and Synthesis of Recognition Molecules, Angew. Chem. Int. Ed., 56(2017) 16328-32.
[4] Y. Jiang, M. Shi, Y. Liu, S. Wan, C. Cui, L. Zhang, et al., Aptamer/AuNP Biosensor for Colorimetric Profiling of Exosomal Proteins, Angew. Chem. Int. Ed., 56(2017) 11916-20.
[5] L. Liu, F. Zhao, W. Liu, T. Zhu, J.Z.H. Zhang, C. Chen, et al., An Electrochemical Biosensor with Dual Signal Outputs: Toward Simultaneous Quantification of pH and O_2 in the Brain upon Ischemia and in a Tumor during Cancer Starvation Therapy, Angew. Chem. Int. Ed., 56(2017) 10471-5.
[6] Y. Luo, L. Zhang, W. Liu, Y. Yu, Y. Tian, A Single Biosensor for Evaluating the Levels of Copper Ion and L-Cysteine in a Live Rat Brain with Alzheimer's Disease, Angew. Chem. Int. Ed., 127(2015) 14259-62.
[7] C. Ding, Y. Tian, Gold nanocluster-based fluorescence biosensor for targeted imaging in cancer cells and ratiometric determination of intracellular pH, Biosens. Bioelectron., 65(2015) 183–190.
[8] A. Barati, M. Shamsipur, H. Abdollahi, Carbon dots with strong excitation-dependent fluorescence changes towards pH. Application as nanosensors for a broad range of pH, Anal Chim Acta., 931(2016) 25-33.
[9] L. Ding, H. Yang, S. Ge, J. Yu, Fluorescent carbon dots nanosensor for label-free determination of vitamin B12 based on inner filter effect, Spectrochim. Acta, Part A, 193 (2018) 305–309.
[10] SM. Zhang, WC. Willett, J. Selhub, DJ. Hunter, EL. Giovannucci, MD. Holmes, et al., Plasma Folate, Vitamin B6, Vitamin B12, Homocysteine, and Risk of Breast Cancer, J Natl Cancer Inst, 95(2003) 373-380.
[11] S. Kalytchuk, K. Poláková, Y. Wang, J.P. Froning, K. Cepe, A.L. Rogach, et al., Carbon Dot Nanothermometry: Intracellular Photoluminescence Lifetime Thermal Sensing, ACS Nano, 11(2017) 1432-42.
[12] J. Wang, X. Wang, H. Tang, Z. Gao, S. He, J. Li, et al., Ultrasensitive electrochemical detection of tumor cells based on multiple layer CdS quantum dots-functionalized polystyrene microspheres and graphene oxide – polyaniline composite, Biosens. Bioelectron., 100(2018) 1-7.
[13] L.V. Nair, D.S. Philips, R.S. Jayasree, A. Ajayaghosh, A Near-Infrared Fluorescent Nanosensor (AuC@Urease) for the Selective Detection of Blood Urea, Small, 9(2013) 2673-7.
[14] J. Hatai, L. Motiei, D. Margulies, Analyzing Amyloid Beta Aggregates with a Combinatorial Fluorescent Molecular Sensor, J. Am. Chem. Soc., 139(2017) 2136-9.
[15] F. Li, C. Lei, Q. Shen, L. Li, M. Wang, M. Guo, et al., Analysis of copper nanoparticles toxicity based on a stress-responsive bacterial biosensor array, Nanoscale, 5(2013) 653-62.
[16] B. Luan, S. Zhou, D. Wang, R. Zhou, Detecting Interactions between Nanomaterials and Cell Membranes by Synthetic Nanopores, ACS Nano, 11(2017) 12615-23.
[17] S.K. Misra, I. Srivastava, I. Tripathi, E. Daza, F. Ostadhossein, D. Pan, Macromolecularly “Caged” Carbon Nanoparticles for Intracellular Trafficking via Switchable Photoluminescence, J. Am. Chem. Soc., 139(2017) 1746-9.
[18] L.-L. Li, J. Ji, R. Fei, C.-Z. Wang, Q. Lu, J.-R. Zhang, et al., A Facile Microwave Avenue to Electrochemiluminescent Two-Color Graphene Quantum Dots, Adv. Funct. Mater., 22(2012) 2971-9.
[19] K.M. Chan, W. Xu, H. Kwon, A.M. Kietrys, E.T. Kool, Luminescent Carbon Dot Mimics Assembled on DNA, J. Am. Chem. Soc., 139(2017) 13147-55.
[20] S. Zhu, Q. Meng, L. Wang, J. Zhang, Y. Song, H. Jin, et al., Highly photoluminescent carbon dots for multicolor patterning, sensors, and bioimaging, Angew. Chem. Int. Ed., 52(2013) 3953-7.
[21] G.A.M. Hutton, B. Reuillard, B.C.M. Martindale, C.A. Caputo, C.W.J. Lockwood, J.N. Butt, et al., Carbon Dots as Versatile Photosensitizers for Solar-Driven Catalysis with Redox Enzymes, J. Am. Chem. Soc., 138(2016) 16722-30.
[22] J. Liu, N. Wang, Y. Yu, Y. Yan, H. Zhang, J. Li, et al., Carbon dots in zeolites: A new class of thermally activated delayed fluorescence materials with ultralong lifetimes, Sci Adv., 3(2017) 5.
[23] J. Ge, M. Lan, B. Zhou, W. Liu, L. Guo, H. Wang, et al., A graphene quantum dot photodynamic therapy agent with high singlet oxygen generation, Nat Commun, 5(2014) 4596.
[24] V. Georgakilas, J.A. Perman, J. Tucek, R. Zboril, Broad Family of Carbon Nanoallotropes: Classification, Chemistry, and Applications of Fullerenes, Carbon Dots, Nanotubes, Graphene, Nanodiamonds, and Combined Superstructures, Chem. Rev., 115(2015) 4744-822.

[25] L. Cao, X. Wang, M.J. Meziani, F. Lu, H. Wang, P.G. Luo, et al., Carbon Dots for Multiphoton Bioimaging, J. Am. Chem. Soc., 129(2007) 11318-9.
[26] C. Rizzo, F. Arcudi, L. Đorđević, N.T. Dintcheva, R. Noto, F. D'Anna, et al., Nitrogen-Doped Carbon Nanodots-Ionogels: Preparation, Characterization, and Radical Scavenging Activity, ACS Nano, 12(2018) 1296-305.
[27] X. Xu, R. Ray, Y. Gu, H.J. Ploehn, L. Gearheart, K. Raker, et al., Electrophoretic Analysis and Purification of Fluorescent Single-Walled Carbon Nanotube Fragments, J. Am. Chem. Soc., 126(2004) 12736-7.
[28] P. Russo, R. Liang, E. Jabari, E. Marzbanrad, E. Toyserkani, Y.N. Zhou, Single-step synthesis of graphene quantum dots by femtosecond laser ablation of graphene oxide dispersions, Nanoscale, 8(2016) 8863-77.
[29] Y. Xu, J. Liu, J. Zhang, X. Zong, X. Jia, D. Li, et al., Chip-based generation of carbon nanodots via electrochemical oxidation of screen printed carbon electrodes and the applications for efficient cell imaging and electrochemiluminescence enhancement, Nanoscale, 7(2015) 9421-6.
[30] A. Rahy, C. Zhou, J. Zheng, S.Y. Park, M.J. Kim, I. Jang, et al., Photoluminescent carbon nanoparticles produced by confined combustion of aromatic compounds, Carbon, 50(2012) 1298-302.
[31] F. Yuan, Z. Wang, X. Li, Y. Li, Z.a. Tan, L. Fan, et al., Bright Multicolor Bandgap Fluorescent Carbon Quantum Dots for Electroluminescent Light-Emitting Diodes, Adv. Mater., 29(2017) 1604436-n/a.
[32] J. Wang, C.-F. Wang, S. Chen, Amphiphilic Egg-Derived Carbon Dots: Rapid Plasma Fabrication, Pyrolysis Process, and Multicolor Printing Patterns, Angew. Chem. Int. Ed., 51(2012) 9297-301.
[33] C.-z. Li, K. Vandenberg, S. Prabhulkar, X. Zhu, L. Schneper, K. Methee, et al., Paper based point-of-care testing disc for multiplex whole cell bacteria analysis, Biosens. Bioelectron., 26(2011) 4342-8.
[34] T. Kilic, A. Erdem, M. Ozsoz, S. Carrara, microRNA biosensors: Opportunities and challenges among conventional and commercially available techniques, Biosens. Bioelectron., 99(2018) 525-46.
[35] L. Xu, W. Liang, Y. Wen, L. Wang, X. Yang, S. Ren, et al., An ultrasensitive electrochemical biosensor for the detection of mecA gene in methicillin-resistant Staphylococcus aureus, Biosens. Bioelectron., 99(2018) 424-30.
[36] X. Huang, F. Zhang, L. Zhu, K.Y. Choi, N. Guo, J. Guo, et al., Effect of Injection Routes on the Biodistribution, Clearance, and Tumor Uptake of Carbon Dots, ACS Nano, 7(2013) 5684-93.
[37] F. Li, T. Li, C. Sun, J. Xia, Y. Jiao, H. Xu, Selenium-Doped Carbon Quantum Dots for Free-Radical Scavenging, Angew. Chem. Int. Ed., 56(2017) 9910-4.
[38] M. Algarra, M. Perez-Martin, M. Cifuentes-Rueda, J. Jimenez-Jimenez, J.C.G. Esteves da Silva, T.J. Bandosz, et al., Carbon dots obtained using hydrothermal treatment of formaldehyde. Cell imaging in vitro, Nanoscale, 6(2014) 9071-7.
[39] H. Li, C. Liang, W. Chen, J.-M. Jin, S.-Y. Tang, Y. Tao, Monitoring in vivo metabolic flux with a designed whole-cell metabolite biosensor of shikimic acid, Biosens. Bioelectron., 98(2017) 457-65.
[40] H. Huang, C. Li, S. Zhu, H. Wang, C. Chen, Z. Wang, et al., Histidine-Derived Nontoxic Nitrogen-Doped Carbon Dots for Sensing and Bioimaging Applications, Langmuir, 30(2014) 13542-8.
[41] J. Joseph, A.A. Anappara, Microwave-assisted hydrothermal synthesis of UV-emitting carbon dots from tannic acid, New J. Chem., 40(2016) 8110-7.
[42] M. Zawadzki, Synthesis of nanosized and microporous zinc aluminate spinel by microwave assisted hydrothermal method (microwave–hydrothermal synthesis of ZnAl2O4), Solid State Sci., 8(2006) 14-8.
[43] M. Shim, N.W. Shi Kam, R.J. Chen, Y. Li, H. Dai, Functionalization of Carbon Nanotubes for Biocompatibility and Biomolecular Recognition, Nano Lett., 2(2002) 285-8.
[44] A. Sadezky, H. Muckenhuber, H. Grothe, R. Niessner, U. Pöschl, Raman microspectroscopy of soot and related carbonaceous materials: Spectral analysis and structural information, Carbon, 43(2005) 1731-42.
[45] S.-J. Jeon, T.-W. Kang, J.-M. Ju, M.-J. Kim, J.H. Park, F. Raza, et al., Modulating the Photocatalytic Activity of Graphene Quantum Dots via Atomic Tailoring for Highly Enhanced Photocatalysis under Visible Light, Adv. Funct. Mater., 26(2016) 8211-9.
[46] W. Kwon, G. Lee, S. Do, T. Joo, S.-W. Rhee, Size-Controlled Soft-Template Synthesis of Carbon Nanodots toward Versatile Photoactive Materials, Small, 10(2014) 506-13.
[47] X.-W. Hua, Y.-W. Bao, H.-Y. Wang, Z. Chen, F.-G. Wu, Bacteria-derived fluorescent carbon dots for microbial live/dead differentiation, Nanoscale, 9(2017) 2150-61.
[48] S. Qu, X. Wang, Q. Lu, X. Liu, L. Wang, A Biocompatible Fluorescent Ink Based on Water - Soluble Luminescent Carbon Nanodots, Angew. Chem. Int. Ed., 51(2012) 12215-8.

[49] C. Wang, Z. Xu, H. Cheng, H. Lin, M.G. Humphrey, C. Zhang, A hydrothermal route to water-stable luminescent carbon dots as nanosensors for pH and temperature, Carbon, 82(2015) 87-95.
[50] C. Shen, Y. Sun, J. Wang, Y. Lu, Facile route to highly photoluminescent carbon nanodots for ion detection, pH sensors and bioimaging, Nanoscale, 6(2014) 9139-47.
[51] J. B. Punuri, M. R. Ashok, D. Mukesh, Synthesis and characterization of biocompatible carbon-gold (C-Au) nanocomposites and their biomedical applications as an optical sensor for creatinine detection and cellular imaging, Sens. Actuators, B., 264(2018) 468.
[52] Z. Gao, L. Wang, R. Su, R. Huang, W. Qi, Z. He, A carbon dot-based "off–on" fluorescent probe for highly selective and sensitive detection of phytic acid, Biosens. Bioelectron., 70(2015) 232-8.
[53] C. Chen, J. Li, C. Li, H. Huang, C. Liang, Y. Lou, et al., Facile Synthesis of Water-Soluble YVO4:Eu Nanoparticles for Cu2+ Detection in Aqueous Solution, ChemistrySelect, 1(2016) 1417-20.

Fig. 1 TEM micrographs of s-N-CDs (inset with a higher magni-fication). (b) XRD pattern of s-N-CDs, (c) Raman spectrum of s-N-CDs, and (d) FTIR spectrum of s-N-CDs and saccharomycetes.
Fig. 2 XPS spectrum of dried s-N-CDs. (a) survey spectrum. The high-resolution XPS peaks of (b) C 1s. (c) N 1s. (d) O 1s
Fig. 3 (a) UV absorption and (inset) optical images under (left) daylight, (intermediate) UV light, (right) printed patterns (λ_{ex}=365, UV lamp) (b) Excitation−emission color map (c) The corresponding calculated CIE coordinate diagram emissions from the samples shown in parts (b). (d) decay curve of s-N-CDs (λ_{ex} = 380 nm, λ_{em} = 460 nm).
Fig. 4 Normalized color plot of fluorescence spectra (a), photostability (b), of the s-N-CDs under the UV irradiation (λ_{ex}=365 nm). Normalized color plot of fluorescence spectra (c), photostability (d), of the s-N-CDs at temperatures from 2 to 80°C. Normalized color plot of fluorescence spectra (e), photostability (f), at PBS concentration between 0.1 and 1M (pH = 7.4)
Fig. 5 (a) Normalized color plots of fluorescence spectra of s-N-CDs solutions with different pH values (from 2 to 14). (b) Optical images under UV lamp at pH = 13 (left) and pH = 2 (right). (c) Normalized color plots of the reversible PL intensity of s-N-CDs solutions with varying pH between 2 and 13. (d) Corresponding photostability of reversible fluorescence intensity of s-N-CDs.
Fig. 6 Normalized color plot of PL lifetimes (a), Decay curves (b), corresponding PL lifetimes (c) of the s-N-CDs at temperatures from 2 to 80°C (λ_{em}= 460 nm). Normalized color plot of PL lifetimes (d), Decay curves (e), corresponding PL lifetimes (f) of the s-N-CDs at pH from 1 to 14.
Fig. 7 Laser confocal microscopic images of A549 cells after incubation with s-N-CDs at pH 6.0 (a), 7.0 (b), and 8.0 (c) (from left to right: fluorescent image excited with a 405 nm laser, brightfield, and the merged images, respectively.)
Fig. 8 (a) Normalized color plot of fluorescence spectra of the s-N-CDs solutions with vitamins (VB 1, VB 3, VB 5, VB 6, VB 7 and VB 12). (b) corresponding fluorescence spectra. (c) Normalized color plot of fluorescence spectra of the s-N-CDs solutions with various concentrations of VB 12 (0-100 μM), (d) corresponding fluorescence spectra.

Highlights

- a simple method was explored with environmental-friendly raw materials for carbon dots preparation;
- a new explanation was proposed to the change of fluorescence intensity with pH, which could provide new rational for design of pH biosensors;
- as a cobalamin detection sensor, the carbon dots present a detection resolution up to 2.19 μM.

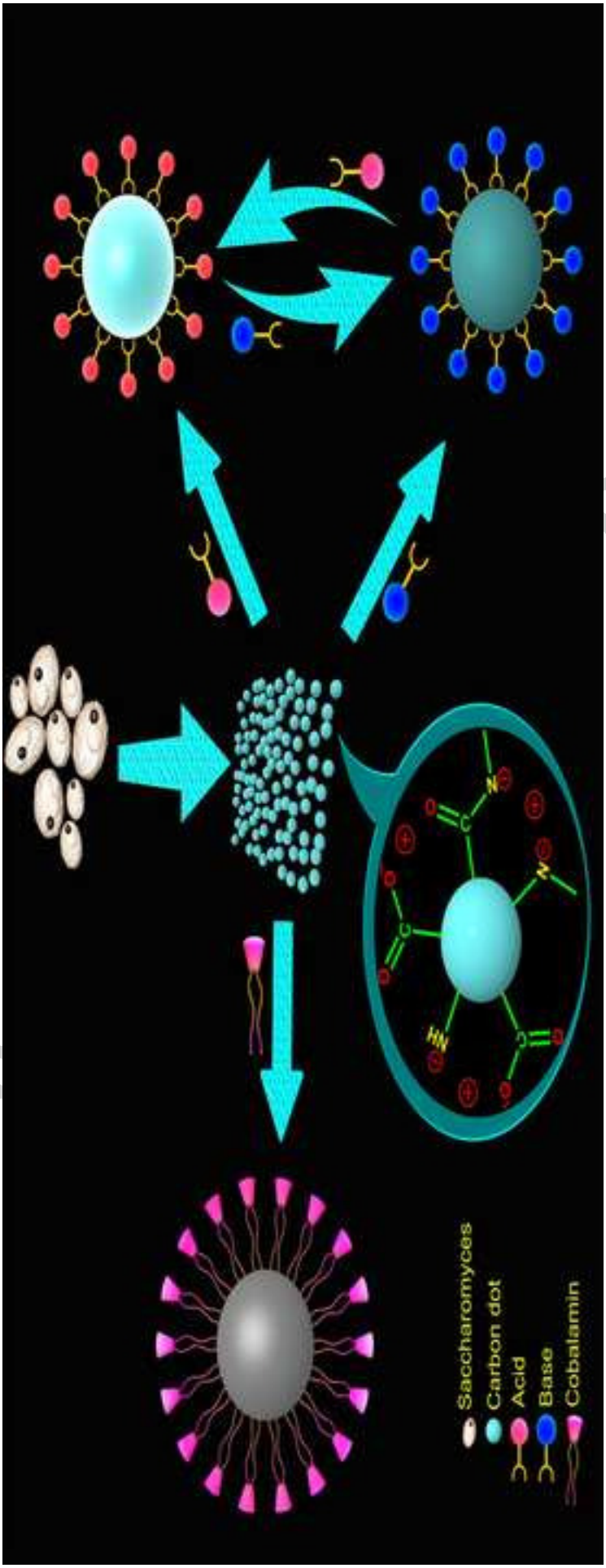

*Graphical Abstract (for review)

Figure

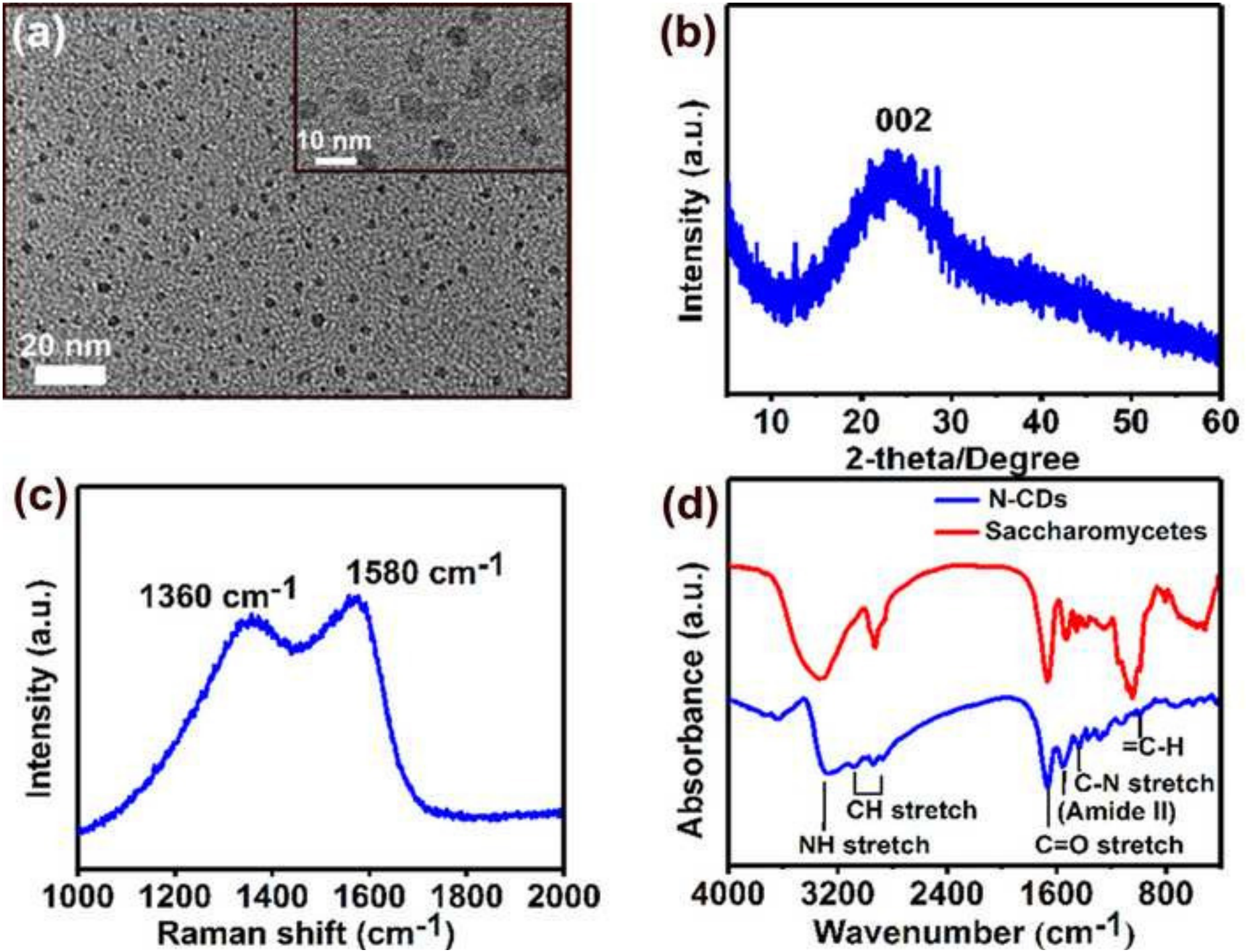

Figure

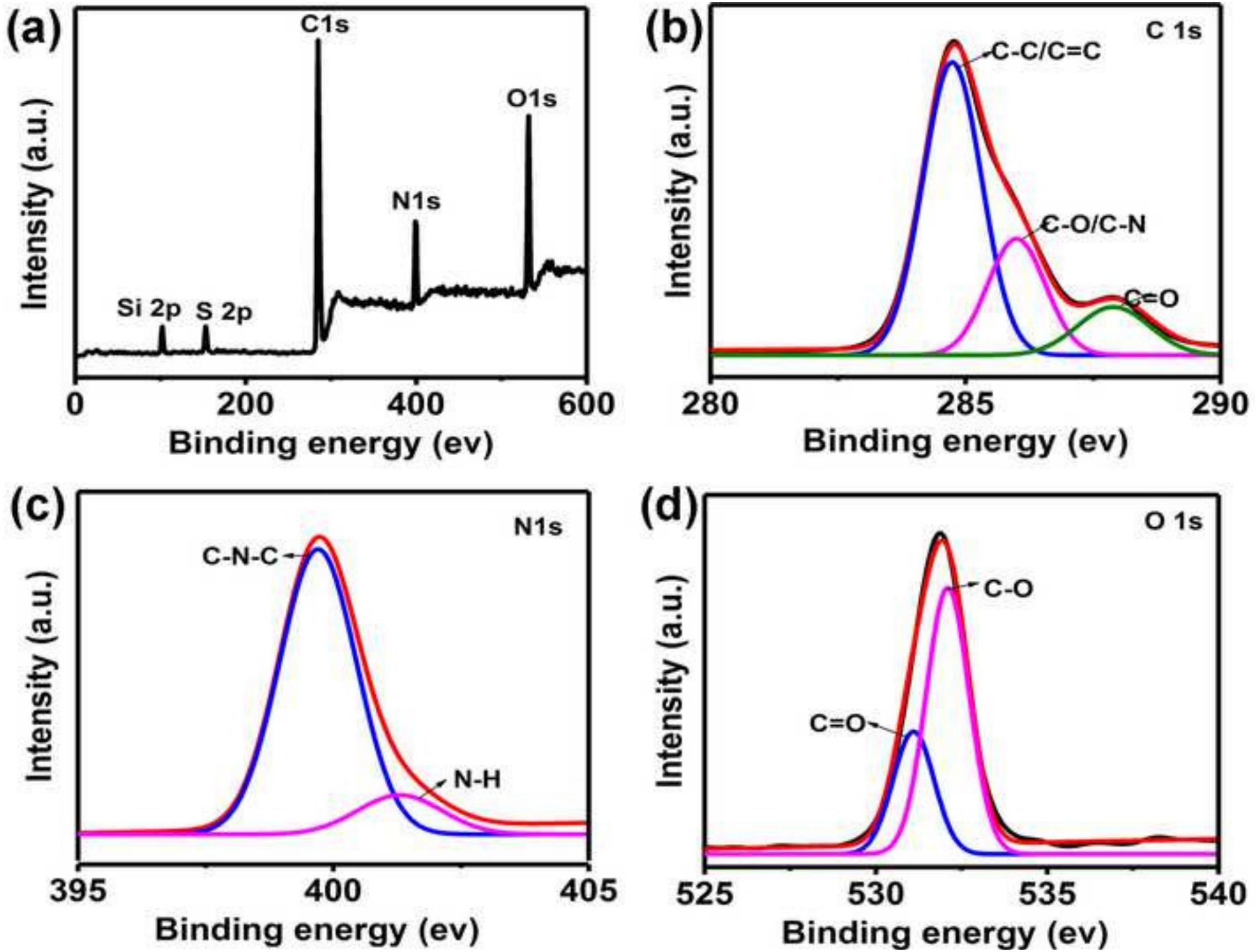

Figure

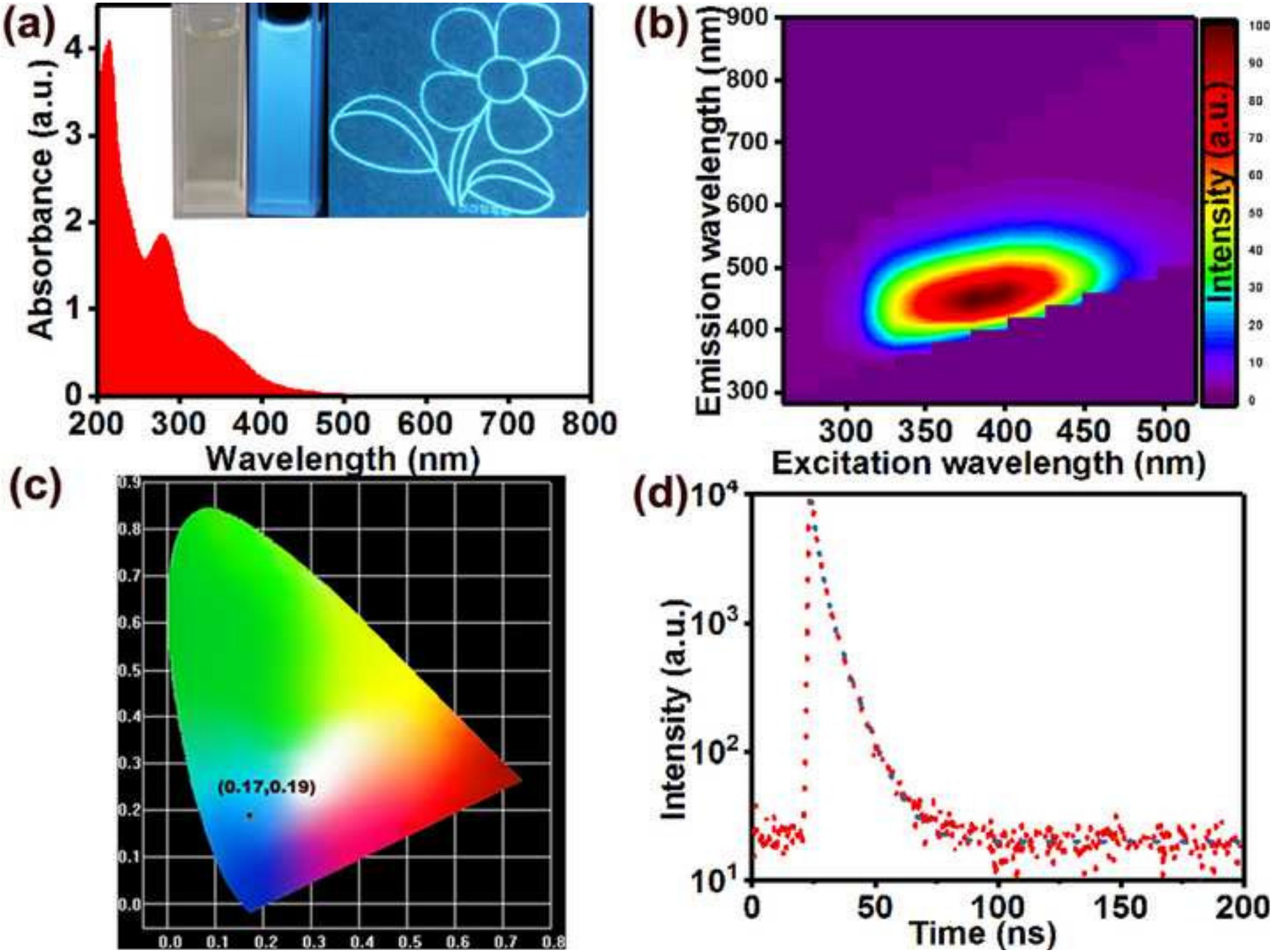

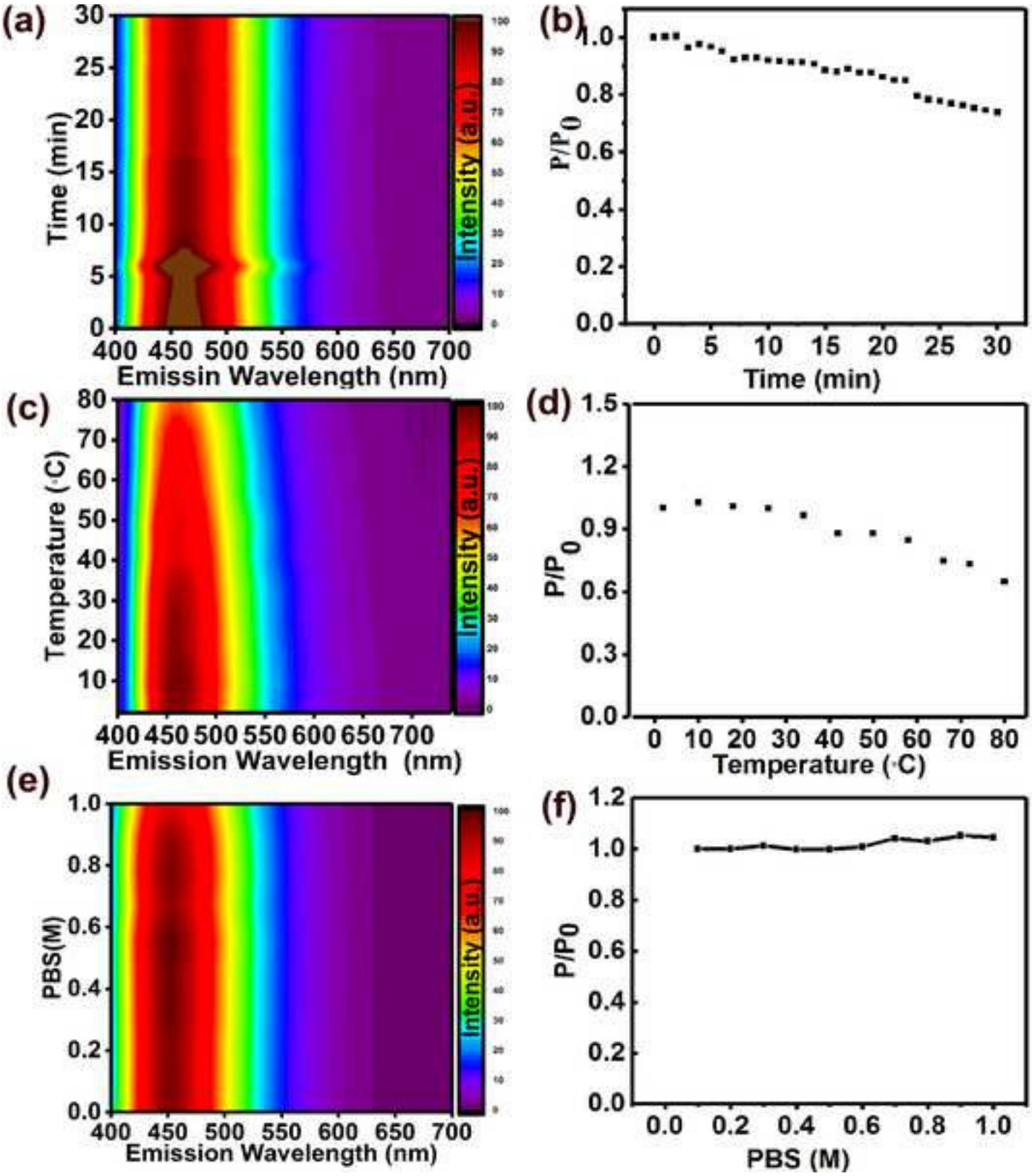

Figure

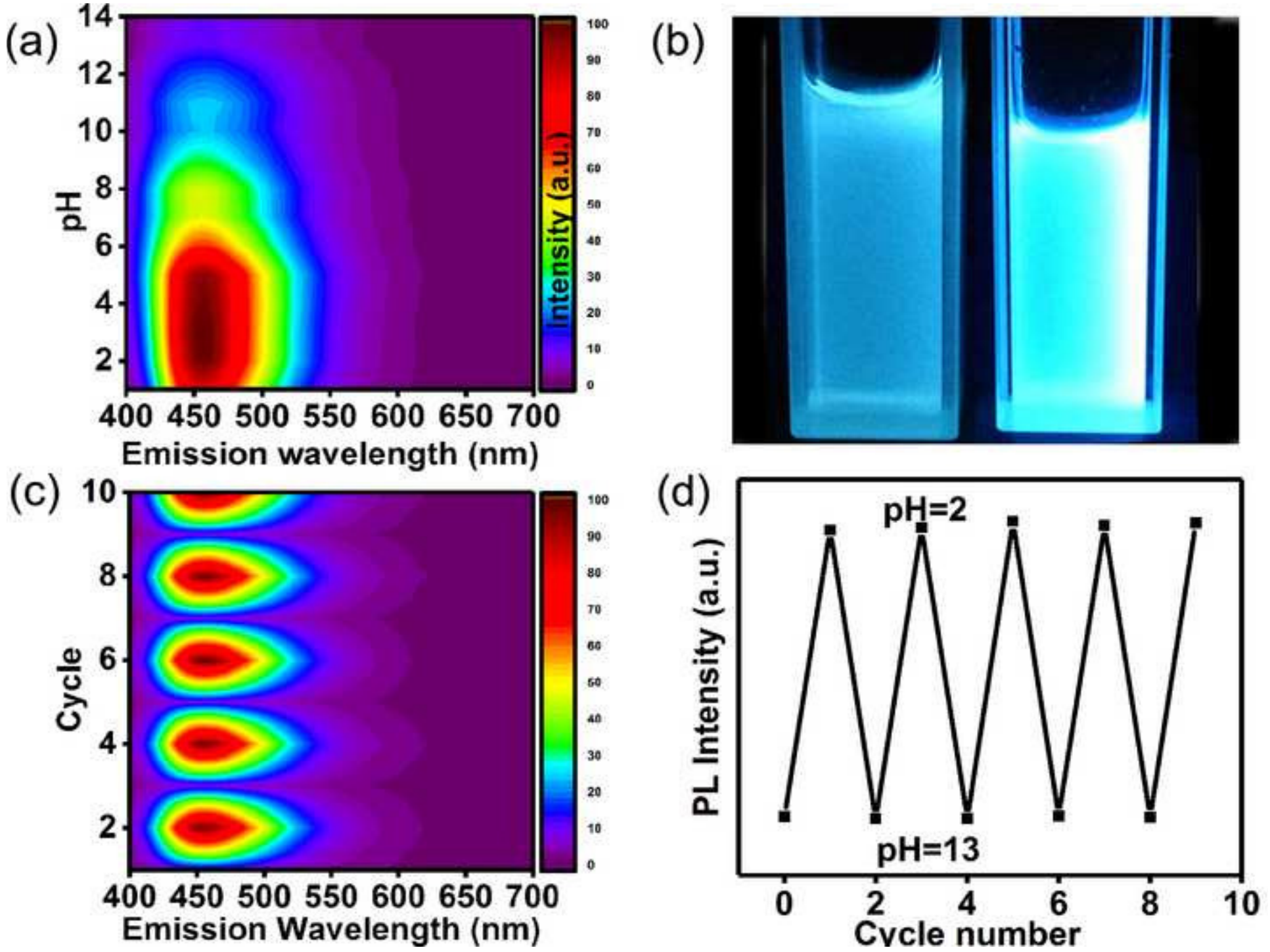

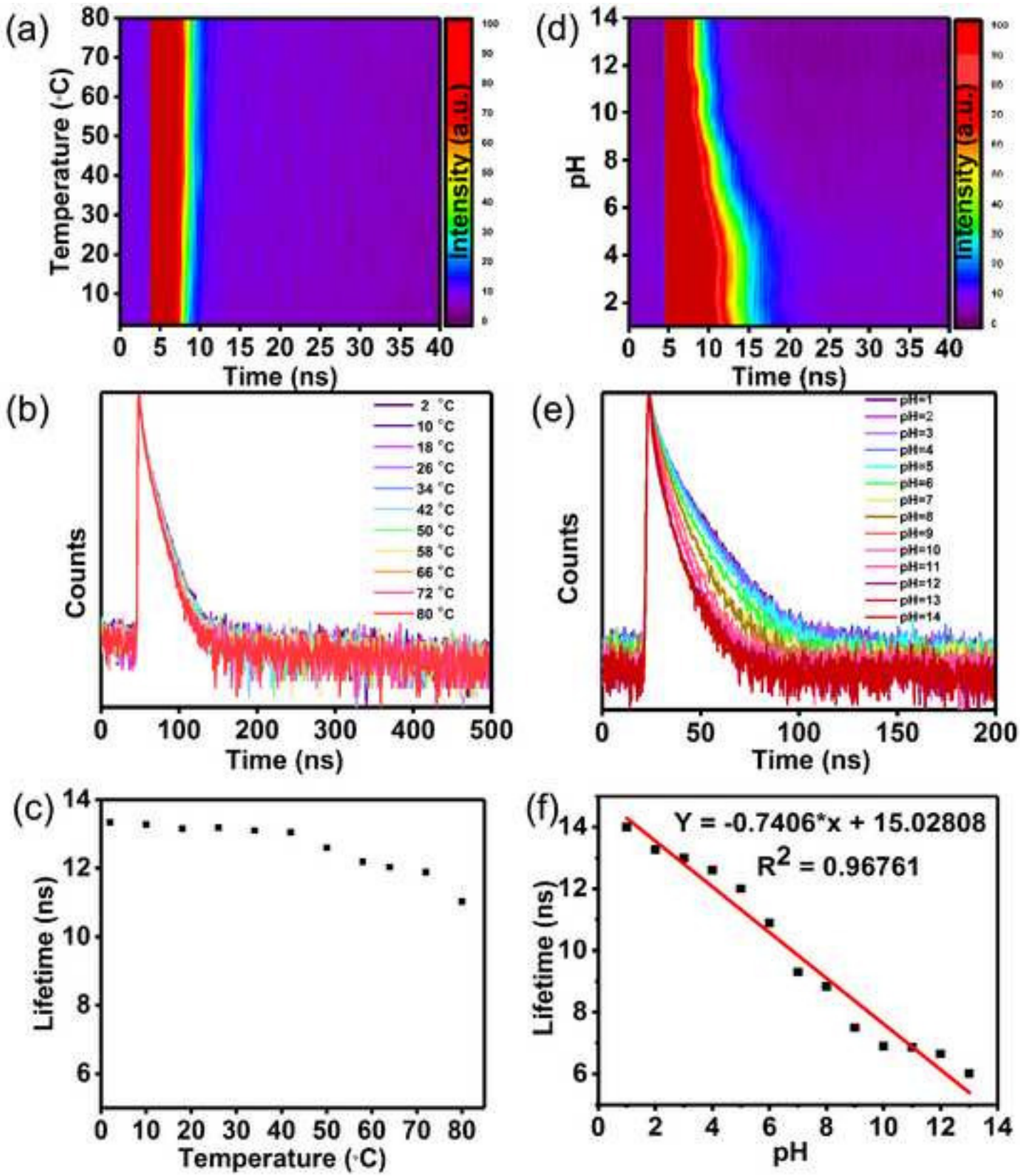

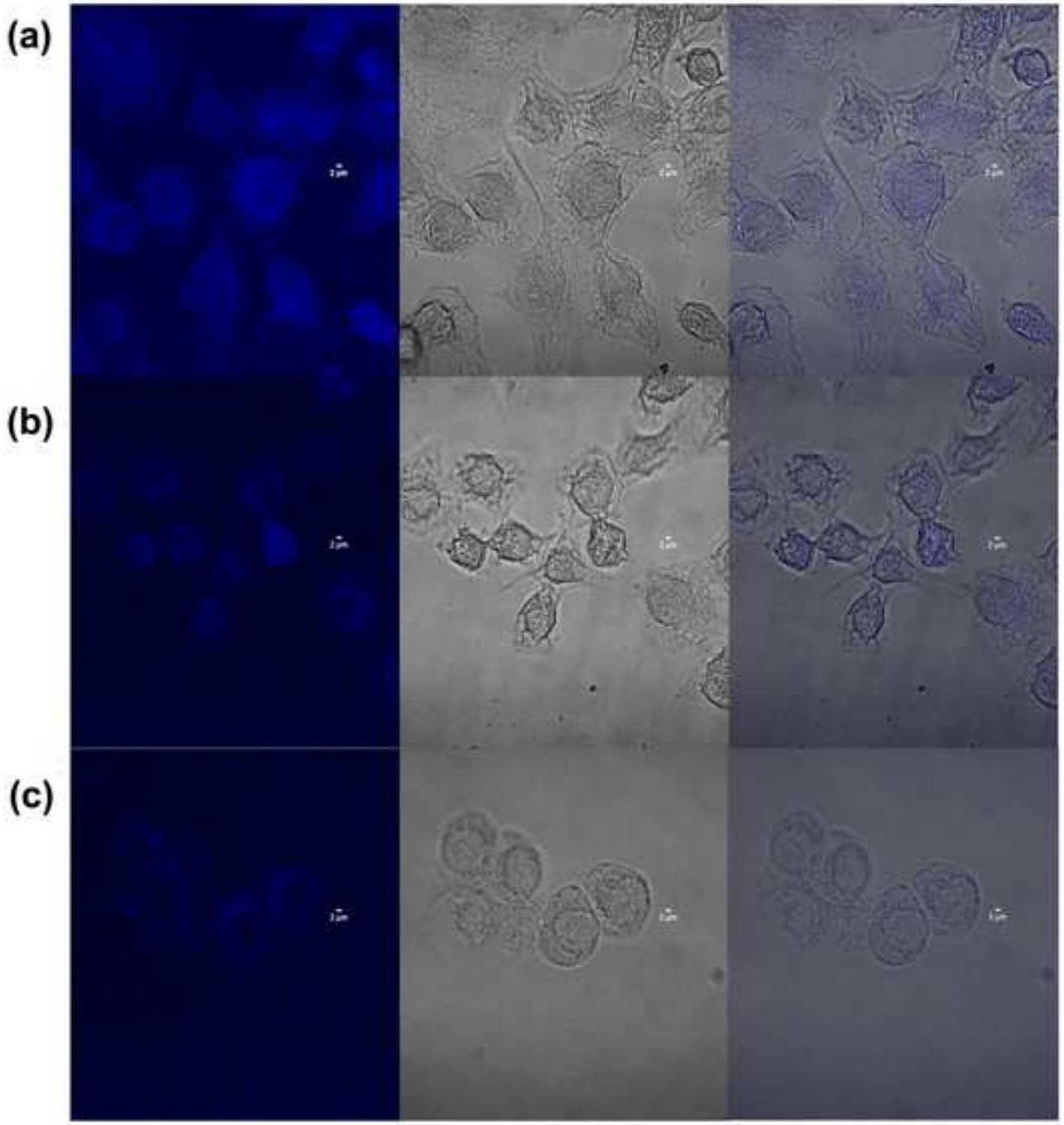

Figure